Lecture, held at Kyushu University.

Reprinted: 05-12-2000
Website: www.shipmotions.nl

Report 1237, 27 October 2000,
Delft University of Technology,
Ship Hydromechanics Laboratory,
Mekelweg 2, 2628 CD Delft,
The Netherlands.

Fluid Tanks and Ship Motions

J.M.J. Journée,

Abstract

This presentation deals with the non-viscous fluid motions in (cargo) tanks on a ship and its effect on the motions of the ship in waves. Research results, presented by the author and his colleagues on three International Conferences on Stability of Ships and Ocean Structures (1994, 1997 and 2000), will be summarized and discussed here.
When a double bottom tank, a cargo tank or a space in a rolling vessel contains a fluid, gravity waves will appear at the surface of this fluid. These gravity waves will cause exciting roll moments on the vessel. At lower water depths, resonance frequencies can be obtained with high wave amplitudes. A hydraulic jump or bore, which is a strongly non-linear phenomenon, travels periodically back and forth between the walls of the tank. A theory, based on gas-dynamics for the shock wave in a gas flow, has been used to describe the motions of the fluid in the frequency domain. At higher water depths, the behavior of the fluid tends to be more linear and the linear potential theory can be used to describe the motions of the fluid in the tank. Experimental data on forced oscillations of free-surface anti-rolling tanks and cargo tanks have been used to verify the theoretical approaches. A ship model equipped with liquid cargo tanks has been tested in beam waves at zero forward speed. Measured roll data have been compared with results of strip theory calculations in the frequency domain.
Also, the ship's motion behavior in the time-domain after a collision damage and the associated stability characteristics during the intermediate stages of flooding have been investigated. A mathematical model, describing the ship's motions due to flooding in the time domain, has been developed. For validation, a large number of tests were held with two models on a systematic basis. The effects of initial metacentric height, ingress area, initial heeling angle, presence of longitudinal bulkheads and cross ducts, reduction of permeability's and down-flooding on capsizing have been examined. Some results are presented here in this lecture. Considerations with respect to the intermediate stages of flooding and the initial conditions are given.

1 Introduction

When a tank that contains a fluid with a free surface is forced to carry out roll oscillations, resonance frequencies can be obtained with high wave amplitudes at lower water depths. Under these circumstances a hydraulic jump or bore is formed, which travels periodically back and forth between the walls of the tank. This

hydraulic jump can be a strongly non-linear phenomenon. A theory, based on gas-dynamics for the shock wave in a gas flow under similar resonance circumstances, as given by Verhagen and Van Wijngaarden (1965), has been adapted and used to describe the motions of the fluid. For low and high frequencies and frequencies near to the natural frequency, different approaches have been used. A calculation routine has been made to connect these regions. Experimental data on the behavior of the fluid in free-surface anti-rolling tanks, obtained from Van den Bosch and Vugts (1966), have been used to validate this approach.
At higher water depths, the behavior of the fluid tends to be more linear. Then, the linear potential theory with the pulsating source method of Frank (1967) - as generally used in strip theory ship motion computer codes - has been used to describe the motions of the fluid in the tank. Forced roll oscillation tests were carried out with a 2-D model of a cargo tank of a LNG carrier. For a wide range of frequencies and filling levels, measured exciting tank moments have been compared with theoretical predictions. A ship model - equipped with three of these liquid cargo tanks - was tested in beam waves at zero forward speed. Several filling levels and two regular wave amplitudes were used to investigate the effect on the non-linear roll behavior of the ship in the frequency domain. Measured roll data were compared with the results of 2-D potential calculations.

The dynamic behavior of ships during sudden ingress of water - after a collision at the side - has been investigated in the time domain. For this purpose, the roll motions of two models of typical Ro-Ro vessels were measured on time basis.
First, a series of model experiments has been carried out with a Ro-Ro vessel with a block coefficient of about 0.62, named here "Ferry-62". The transverse bulkhead between the two engine rooms was at half-length of the collision gap. From the two amidships engine rooms until aft, the ship was divided in compartments by transverse bulkheads only. Forward of the engine rooms, the ship was subdivided by two longitudinal bulkheads at one-fifth of the breadth from the hull, transverse bulkheads in the side at small mutual distances and no bulkheads in the center part.
Then, similar experiments have been carried out with another Ro-Ro vessel with a block coefficient of about 0.72, named here "Ferry-72". This ship had a quite different watertight division. Below the Ro-Ro deck, two longitudinal bulkheads subdivide the ship over the full length at one-fifth of the breadth from the hull. The length of the wing compartments was rather small, while the transverse bulkheads in the center part were located at a much larger distance. To avoid large heeling angles in case of a lateral collision, cross ducts in the double bottom will transfer the incoming seawater to the other side of the vessel (equalizing arrangement).
For both models, the experiments were carried out at 3 initial metacentric heights and 4 collision gaps. Research results were presented by Journée, Vermeer and Vredeveldt (in alphabetic order) at three International Conferences on Stability of Ships and Ocean Structures (1994, 1997 and 2000).
A number of experimental results is presented here and discussed. Also, some comparisons of experimental data with time domain results of theoretical approximations of the dynamic behavior of the models during ingress of water are given.

2 Frequency Domain Approach

Observe a rectangular tank with length l and breadth b, which has been filled until water level h with fluid with a mass density r.
The distance of the tank bottom above the center of gravity of the vessel is s.
Figure 1 shows a 2-D sketch of this tank with the axis system and notations.

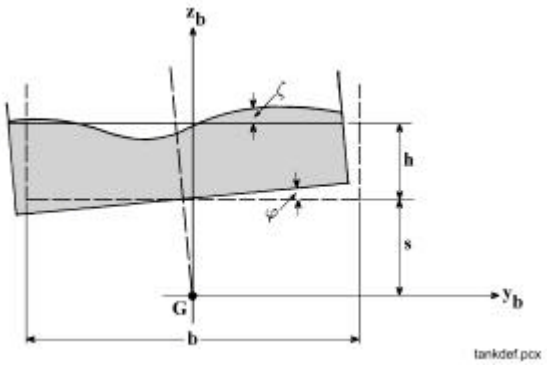

Figure 1 Axis system and Notations

The natural frequency of the surface wave in a harmonic rolling tank appears as the wave length l equals twice the breadth b, so:

$$l_0 = 2 \cdot b .$$

With the wave number and the dispersion relation:

$$k = \frac{2p}{l} \text{ and } w = \sqrt{\frac{p \cdot g}{b} \cdot \tanh\left(\frac{p \cdot h}{b}\right)}$$

it follows for the natural frequency of surface waves in the tank:

$$w_0 = \sqrt{\frac{p \cdot g}{b} \cdot \tanh\left(\frac{p \cdot h}{b}\right)}$$

The roll motions and the exciting moments of an oscillating fluid tank, are defined by:

$$j = j_a \cdot \cos(wt)$$
$$K_t = K_{ta} \cdot \cos(wt + e_{tz})$$

The external roll moment due to a fluid tank, oscillating with a frequency w, can be written as:

$$K_t = a_{4j} \cdot \ddot{j} + b_{4j} \cdot \dot{j} + c_{4j} \cdot j$$

with:

$$a_{4j} = 0$$
$$b_{4j} = \frac{K_{ta}}{w j_a} \cdot \sin e_{tj}$$
$$c_{4j} = \frac{K_{ta}}{j_a} \cdot \cos e_{tj}$$

It is obvious that for a fluid tank, build in the ship, the motions of ship and tank are similar:

$$f_a = j_a \text{ and } w_e = w$$

One can express the roll motion of the ship as well as the tank moment on the ship as:

$$f = f_a \cdot \cos(wt)$$
$$K_t = K_{ta} \cdot \cos(wt + e_{fz} + e_{tz})$$

Then, an additional exciting moment has to be added to the right hand side of the equations of motion for roll:

$$X_{44\,fluid} = a_{44\,fluid} \cdot \ddot{j} + b_{44\,fluid} \cdot \dot{j} + c_{44\,fluid} \cdot j$$

with:

$$a_{44\,fluid} = 0$$
$$b_{44\,fluid} = \frac{K_{ta}}{w_e f_a} \cdot \sin e_{tj}$$
$$c_{44\,fluid} = \frac{K_{ta}}{f_a} \cdot \cos e_{tj}$$

This holds that the anti-roll coefficients $a_{44\,fluid}$, $b_{44\,fluid}$ and $c_{44\,fluid}$ have to be subtracted from the coefficients a_{44}, b_{44} and c_{44} in the left-hand side of the equation of motion for roll.

2.1 Shallow Water Theory

Verhagen and Van Wijngaarden (1965) have investigated the shallow water wave loads in a rolling rectangular container, with the

center of rotation at the bottom of the container. Their expressions for the internal wave loads are rewritten and modified in this paper, to be useful for any arbitrary vertical position of the center of rotation. For low and high frequencies and frequencies near to the natural frequency, different approaches have been used. A calculation routine has been made to connect these three regions.

Low and High Frequencies

The harmonic roll motion of the tank in Figure 1 is defined by:

$$f = f_a \cdot \sin(wt)$$

After linearisation, the vertical displacement of the tank bottom is described by:

$$z = z + y \cdot f$$

and the surface elevation of the fluid by:

$$z = s + h + z$$

Relative to the bottom of the tank, the linearised surface elevation of the fluid is described by:

$$x = h + z - y \cdot f$$

Using the shallow water theory, the continuity and momentum equations are:

$$\frac{\partial x}{\partial t} + v \cdot \frac{\partial x}{\partial y} + x \cdot \frac{\partial v}{\partial y} = 0$$

$$\frac{\partial v}{\partial t} + v \cdot \frac{\partial v}{\partial y} + g \cdot \frac{\partial x}{\partial y} + g \cdot f = 0$$

In these formulations, v denotes the velocity of the fluid in the y-direction and the vertical pressure distribution is assumed to be hydrostatic. Therefore, the acceleration in the z-direction, introduced by the excitation, must be small with respect to the acceleration of gravity g, so:

$$f_a \cdot w^2 \cdot b << g$$

The limits of v will be determined by the excitation velocity in the horizontal direction. Between the surface of the fluid and the bottom of the tank, the velocity of the fluid v varies between v_s and $v_s / \cos kh$ with a mean velocity: v_s / kh. However, in very shallow water v does not vary between the bottom and the surface. When taking the value at the surface, it is required that:

$$v = -(s + h) \cdot \dot{f} \quad \text{at} \quad y = \pm \frac{b}{2}$$

For small values of f_a, the continuity equation and the momentum equation can be given in a linearised form:

$$\frac{\partial x}{\partial t} + h \cdot \frac{\partial v}{\partial y} = 0$$

$$\frac{\partial v}{\partial t} + g \cdot \frac{\partial x}{\partial y} + g \cdot f = 0$$

The solution of the surface elevation x in these equations, satisfying the boundary values for v, is:

$$x = h - \frac{b \cdot w_0 \left\{ 1 + \frac{(s+h) \cdot w^2}{g} \right\}}{p \cdot w \cdot \cos\left(\frac{p \cdot w}{b \cdot w_0} \right)} \cdot$$

$$\cdot \sin\left(\frac{p \cdot w \cdot y}{b \cdot w_0} \right) \cdot f$$

Now, the roll moment follows from the quasi-static moment of the mass of the frozen liquid $r \cdot l \cdot b \cdot h$ and an integration of x over the breadth of the tank:

$$M_f = r \cdot g \cdot l \cdot b \cdot h \cdot \left(s + \frac{h}{2} \right) \cdot f + r \cdot g \cdot l \int_{-b/2}^{+b/2} x \cdot y \cdot dy$$

This delivers the roll moment amplitude for low and high frequencies at small water depths:

$$M_{af} = r \cdot g \cdot l \cdot b \cdot h \cdot \left(s + \frac{h}{2} \right) \cdot f + r \cdot g \cdot l \cdot b^3 \cdot \left\{ 1 + \frac{(s+h) \cdot w^2}{g} \right\} \cdot \left\{ 2 \left(\frac{w_0}{pw} \right)^3 \tan\left(\frac{pw}{2w_0} \right) - \left(\frac{w_0}{pw} \right)^2 \right\} \cdot f_a$$

For very low frequencies, so for the limit value $w \to 0$, this will result into the static moment:

$$M_f = r \cdot g \cdot l \cdot \left\{ b \cdot h \cdot \left(s + \frac{h}{2} \right) + \frac{b^3}{12} \right\} \cdot f$$

The phase lags between the roll moments and the roll motions have not been obtained here. However, they can be set to zero for low frequencies and to $-p$ for high frequencies:

$$e_{M_f f} = 0 \text{ for: } w << w_0$$

$$e_{M_f f} = -p \text{ for: } w >> w_0$$

Natural Frequency Region

For frequencies near to the natural frequency w_0, the expression for the surface elevation of the fluid x goes to infinity. Experiments showed the appearance of a hydraulic jump or a bore at these frequencies. Obviously, then the linearised equations are not valid anymore.

Verhagen and Van Wijngaarden (1965) solved the problem by using the approach in gas dynamics when a column of gas is oscillated at small amplitude, e.g. by a piston. At frequencies near to the natural frequency at small water depths, they found a rolling moment amplitude, defined by:

$$M_{af} = r \cdot g \cdot \frac{l \cdot b^3}{12} \cdot \left(\frac{4}{p} \right)^4 \cdot \sqrt{\frac{2 \cdot f_a \cdot h}{3 \cdot b}} \cdot \left\{ 1 - \frac{p^2 \cdot b \cdot (w - w_0)^2}{32 \cdot g \cdot f_a} \right\}$$

The phase lags between the roll moment and the roll motion at small water depths are given by:

$$e_{M_f f} = -\frac{p}{2} + a \text{ for: } w < w_0$$

$$e_{M_f f} = -\frac{p}{2} - a \text{ for: } w > w_0$$

with:

$$a = 2 \cdot \arcsin\left\{ \sqrt{\frac{p^2 b (w - w_0)^2}{24 g f_a}} \right\} - \arcsin\left\{ \sqrt{\frac{p \ b (w - w_0)^2}{96 g f_a - 3 p^2 b (w - w_0)^2}} \right\}$$

Because that the arguments of the square roots in the expression for $e_{M_f f}$ have to be positive, the limits for the frequency w are at least:

$$w_0 - \sqrt{\frac{24 g f_a}{b p^2}} < w < w_0 + \sqrt{\frac{24 g f_a}{b p^2}}$$

2.2 Potential Theory of Frank

For the calculation of the 2-D potential mass and damping of ship-like cross sections, Frank (1967) considered a cylinder, whose cross section is a simply connected region, which is fully or partly immersed,

horizontally in a previously undisturbed fluid of infinite depth.
The cylinder, as given in Figure 2, is forced into simple harmonic motion with radian frequency w, according to the displacement equation:

$$S^{(m)} = A^{(m)} \cdot \cos wt$$

The superscript m may take on the values 2, 3 and 4, denoting sway, heave and roll motions, respectively. The roll motions are about an axis through a point $(0, y_0)$ in the symmetry plane of the cylinder.
It is assumed that steady state conditions have been attained. The fluid is assumed to be incompressible, non-viscous and irrotational, without any effects of surface tension. The motion amplitudes and velocities are small enough, so that all but the linear terms of the free surface condition, the kinematic boundary condition on the cylinder and the Bernoulli equation may be neglected.

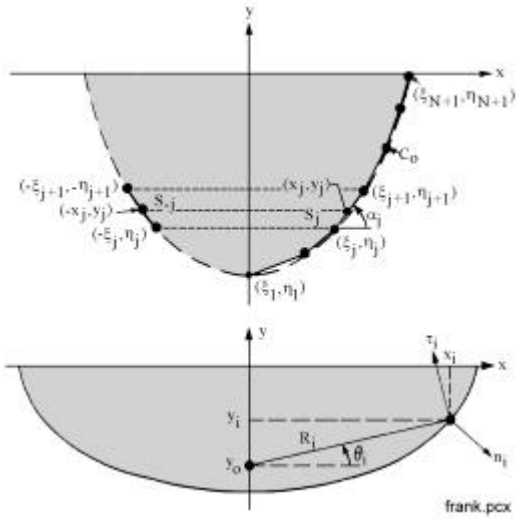

Figure 2 Frank's Axes System

A velocity potential has to be found:

$$\Phi^{(m)} = \mathrm{Re}\left\{f^{(m)}(x, y) \cdot e^{-iwt}\right\}$$

that satifies the equation of Laplace, the symmetry (heave) or anti-symmetry (sway and roll) condition, the free surface condition, the bottom condition, the kinematic boundary condition at the cylindrical surface and the radiation condition. Frank has given a potential function, based on pulsating sources, satisfying the boundary conditions and he defined the complex potential at z of a pulsating point source of unit strength at the point z in the lower half plane, as given in Figure 2.
Take the x-axis to be coincident with the undisturbed free surface. Let the cross sectional contour C_0 of the submerged portion of the cylinder be in the lower half plane and the y-axis, positive upwards, being the axis of symmetry of C_0. Select $N+1$ points (x_i, h_i) of C_0 to lie in the fourth quadrant. Connect these $N+1$ points by successive straight lines. Then, N straight-line segments are obtained which, together with their reflected images in the third quadrant, yield an approximation to the given contour as shown in Figure 2.
The coordinates, length and angle associated with the j^{th} segment are identified by the subscript j, whereas the corresponding quantities for the reflected image in the third quadrant are denoted by the subscript $-j$, so that by symmetry $x_{-j} = x_j$ and $h_{-j} = -h_j$ for $1 \le j \le N+1$. Potentials and pressures are to be evaluated at the midpoint of each segment and for $1 \le i \le N$ the coordinates of the midpoint of the i^{th} segment are:

$$x_i = \frac{x_i + x_{i+1}}{2} \text{ and } y_i = \frac{p_i + h_{i+1}}{2}$$

In the displacement modes, any point on the cylinder moves with the velocity:

$$v^{(2)} = -iA^{(2)}w \cdot \sin wt \text{ for sway}$$
$$v^{(3)} = -iA^{(3)}w \cdot \sin wt \text{ for heave}$$

The length of the i^{th} segment and the angle made by this segment with the positive x-axis are:

$$s_i = \sqrt{(x_{i+1} - x_i)^2 + (h_{i+1} - h_i)^2}$$
$$a_i = \arctan\left\{\frac{h_{i+1} - h_i}{x_{i+1} - x_i}\right\}$$

a_i is defined beteen: $-p/2 \le a_i \le +p/2$.

If the denominator is negative, depending on the sign of the numerator, p has to be added or subtracted, so that a_i will be defined as:

$$-p \le a_i \le +p .$$

The outgoing unit vector normal to the cross section at the i^{th} midpoint (x_i, y_i) is:

$$n_i = +\bar{i} \cdot \sin a_i - \bar{j} \cdot \cos a_i$$

where $\bar{i}$ and $\bar{j}$ are unit vectors in the directions x and y, respectively.

The roll motion is illustrated in Figure 2 and considering a point (x_i, y_i) on C_0 and an inspection of this figure yields:

$$R_i = \sqrt{x_i^{\,2} + (y_i - y_0)^2}$$
$$q_i = \arctan\left(\frac{y_i - y_0}{x_i}\right)$$

In here, q_i is defined as:

$$-p/2 \le q_i \le +p\,2 .$$

If the denominator is negative, depending on the sign of the numerator p has to be added or subtracted, so that q_i will be defined as:

$$-p \le q_i \le +p .$$

By elementary two-dimensional kinematics, the unit vector in the direction q_i is:

$$t_i = -\bar{i} \cdot \sin q_i + \bar{j} \cdot \cos q_i$$

so that:

$$v^{(4)} = S^{(4)} \cdot t_i \cdot R_i$$
$$= -wA^{(4)} R_i \left(\bar{i} \sin q_i - \bar{j} \cos q_i\right) \sin wt$$

The normal components of the velocity at the midpoint of the i^{th} segment (x_i, y_i) are:

$$v_i^{(2)} = -wA^{(2)} \sin a_i \sin wt$$
$$v_i^{(2)} = +wA^{(3)} \cos a_i \sin wt$$
$$v_i^{(2)} = +wA^{(4)} R_i \cdot$$
$$\cdot \left(\sin q_i \sin a_i + \cos q_i \cos a_i\right) \sin wt$$

Defining:

$$n_i^{(m)} = \frac{v_i^{(m)}}{A^{(m)} w \sin wt}$$

then, consistent with the previously mentioned notation, the direction cosines for the three modes of motion are:

$$n_i^{(2)} = -\sin a_i$$
$$n_i^{(3)} = +\cos a_i$$
$$n_i^{(2)} = +\sin q_i \sin a_i + \cos q_i \cos a_i$$

A set of two coupled integral equations are applied by Frank at the midpoints of each of the N segments and is assumed that over an individual segment the complex source strength remains constant, although it varies from segment to segment. Then, the set of coupled integral equations becomes a set of $2N$ linear algebraic equations in the unknowns.

The hydrodynamic pressure $p^{(m)}$ along the cylinder can be obtained from the velocity potential by means of the linearised equation of Bernoulli, where $p_a^{(m)}$ and $p_v^{(m)}$ are the hydrodynamic pressures in phase with the displacement and in phase with the velocity, respectively. The potential as well as the pressure is a function of the oscillation

frequency w. The hydrodynamic force or moment per unit length on the cylinder, necessary to sustain the oscillations, is the integral of $p^{(m)} \cdot n^{(m)}$ over the submerged contour of the cross section C_0.

It is assumed that the pressure at the i^{th} midpoint is the mean pressure for the i^{th} segment, so that the integration reduces to summation, whence:

$$M^{(m)}(w) = 2\sum_{i=1}^{N} p_a{}^{(m)}(x_i, y_i, w) \cdot n_i{}^{(m)} \cdot |s_i|$$

$$N^{(m)}(w) = 2\sum_{i=1}^{N} p_v{}^{(m)}(x_i, y_i, w) \cdot n_i{}^{(m)} \cdot |s_i|$$

for the potential mass and damping forces or moments, respectively.

Frank's method is suitable for the computation of the potential mass and damping of symmetric 2-D shapes, in or below the surface of a fluid. This method has been incorporated in a lot of 2-D ship motion computer codes, all over the world. Starting from the keel point of the cross section, the input data of the off sets have to be read in an upward order. Then, the (outward) normal on the elements of the cross section will be defined to be positive in the direction of the fluid outside the cross section.

Easily, this method can be used to calculate the linear loads due to a potential fluid in an oscillating symmetrical tank too. Starting from the intersection of the free surface with the tank wall, the offsets of the tank have to be read in a downwards order, so in an opposite direction as has to be done for the cross sections of a ship. When doing this, the (inward) normal on the elements of the cross section of the tank will be defined to be positive in the direction of the fluid in the tank. Then, the potential mass and damping of the moving liquid in the tank can be determined. With this, the in-phase part (X_c) and the out-of-phase part (X_s) of the two-dimensional excitation forces and moments about the origin in the water surface of the fluid in a rectangular tank are found:

$$\begin{aligned}
X_{2c} &= w^2 M^{(2)} x_{2a} \\
X_{2s} &= -wN^{(2)} x_{2a} \\
X_{3c} &= w^2 M^{(3)} x_{3a} \\
X_{3s} &= -wN^{(3)} x_{3a} \\
X_{4c} &= w^2 M^{(4)} x_{4a} + \\
&\quad + rg\left\{bh\left(s + \frac{h}{2}\right) + \frac{b^3}{12}\right\} x_{4a} \\
X_{4s} &= -wN^{(4)} x_{4a}
\end{aligned}$$

This approach can be carried out easily with many existing 2-D (and 3-D) ship motions computer programs. However, one should keep in mind that in the calculation method of Frank, the angles a_i and q_i have to be defined well in all four quadrants.

2.3 Validations

Validations were performed to verify the validity of using Frank's pulsating source method for obtaining the moments caused by the motions of liquids in oscillating tanks.

2.3.1 Fully Filled Tank

A fully filled rectangular tank has been observed. It is obvious that the ratio between the effective and the solid mass for sway or heave of the fluid in fully filled tanks is $c_e = 1.0$. The ratio between the effective and the solid moments of inertia for roll of the fluid in a fully filled rectangular tank as a function of the aspect ratio h/b of the tank was given by Graham and Rodriques and published later by Silverman and Abramson (1966) as:

$$c_{e_{ROLL}} = 1 - \frac{4}{1+\frac{h^2}{b^2}} + \frac{768}{\frac{p^5 h}{b}\cdot\left(1+\frac{h^2}{b^2}\right)} \cdot \sum_{n=0}^{\infty}\left\{\frac{\tanh\left[(2n+1)\cdot\frac{ph}{b}\right]}{(2n+1)^5}\right\}$$

This expression had been obtained from results of space vehicle studies carried out by NASA. The contributions of frequencies higher than the first order are very small and can be neglected.
Calculations have been performed with the 2-D computer code SEAWAY of Journée (1999), that includes Frank's pulsating source method. Also, 3-D calculations have been carried out with the DELFRAC computer code of Pinkster (1996). The results are given in Figure 3.

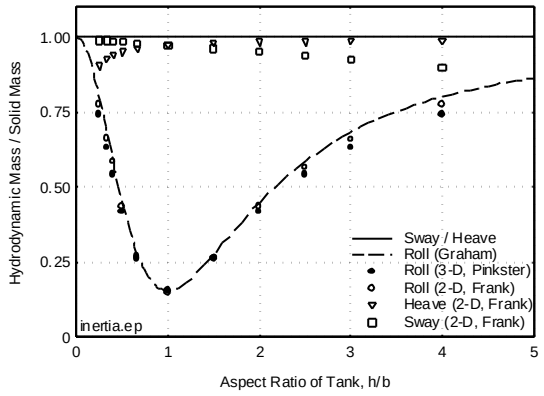

Figure 3 Moment of Inertia of a Fully Filled Tank

Figure 3 shows a fairly good agreement between these results. For small and large aspect ratios deviations can be expected, caused by the limited number of 16 line elements in SEAWAY or 30 panels in DELFRAC on the contour of half the cross section of the tank.

Effects on Ship Motions
Fully filled tanks only affects the mass, the mass moment of inertia and the location of the center of gravity. A change of the natural frequency will be the result.

2.3.2 Free-Surface Tank

A passive free-surface tank can be a very good tool to reduce roll motions, especially at low speeds where anti-roll fins are not effective. This tank has a breadth equal to the ship's breadth and its length is about 1.5 to 2.5 meters, depending on the size of the ship. The roll damping, caused by a passive free-surface tank, is essentially based on the existence of a hydraulic jump or bore in the tank.

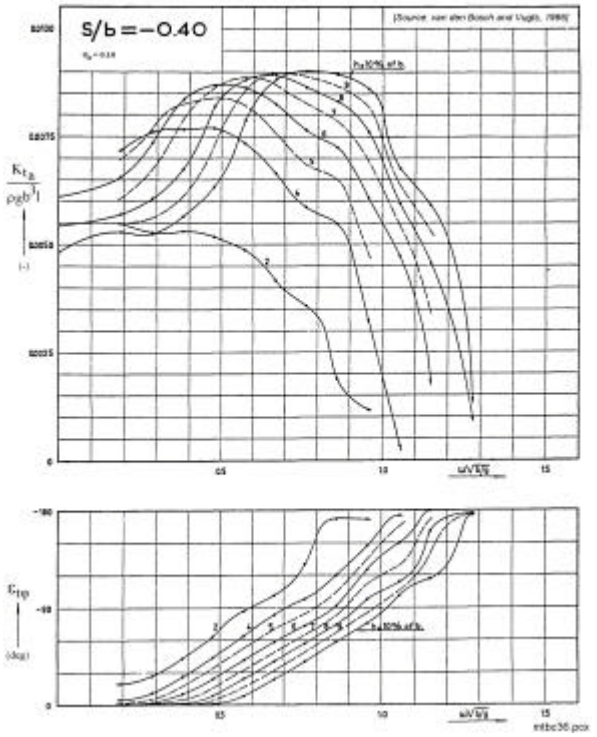

Figure 4 Experimental Data on Anti-Roll Free-Surface Tanks

Van den Bosch and Vugts (1966) have described the physical behavior of passive free-surface tanks, used as an anti-roll device. They assembled extensive quantitative information on the counter-acting moments caused by the water transfer in the tank. In a practical frequency range, they have presented experimental data on the roll moment amplitudes, K_{ta}, and the phase-

shifts of these moments with respect to roll, e_{tz}, for three roll amplitudes (j_a = 0.033, 0.067 and 0.100 rad), four centers of rotation, s, $(-0.40 \le s.b \le +0.20)$ and five water depths, h, $(0.02 \le h/b \le 0.10)$. Figure 4 shows an example of the experimental data.

Figure 5 and Figure 6 show a few comparisons between calculated and measured in and out phase parts of the first harmonic of the roll moments for very small water depths in the tank.

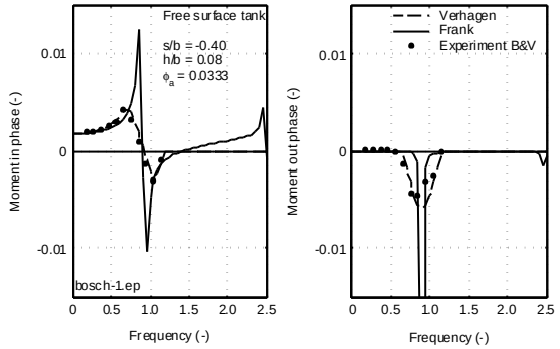

Figure 5 Roll Moments of a Free Surface Tank with Bottom below G

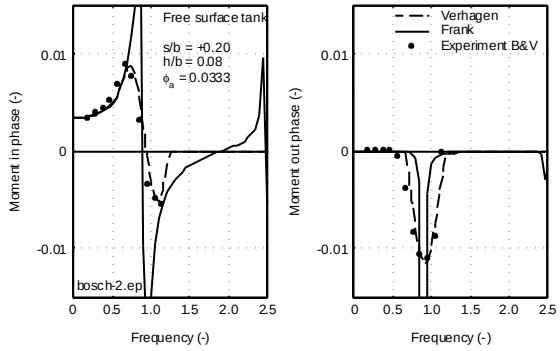

Figure 6 Roll Moments of a Free Surface Tank with Bottom above G

Comparisons are given here for one filling level $(h/b = 0.08)$ and one roll amplitude $(f_a = 0.0333 = 1.9^0)$. Two positions of the bottom with respect to the rotation point, i.e. the center of gravity G of the vessel, have been taken: 40 per cent of the tank width below the axis of rotation $(s/b = -0.40)$ and 20 per cent above it $(s/b = +0.20)$. The roll moment has been made non-dimensional by dividing this moment through $r\,\mathrm{glb}^3$. The non-dimensional frequency parameter has been obtained by dividing the frequency through $\sqrt{g/b}$.

Outside the natural frequency area, the figure shows a good agreement between Frank's method and the experiments. But, for frequencies close to the natural frequency, a very poor prediction has been found. Because of the appearance of a hydraulic jump or a bore at these frequencies, the linearised equations are not valid anymore. The calculated phase lags between the roll moments and the roll motions have a step of 180 degrees at the natural frequency, while the calculated roll moment amplitudes go to infinity.

Because of a distinction between frequencies close to the natural frequency and frequencies far from it, the shallow water method of Verhagen and Van Wijngaarden shows a good prediction at all frequencies.

Effect on Ship Motions

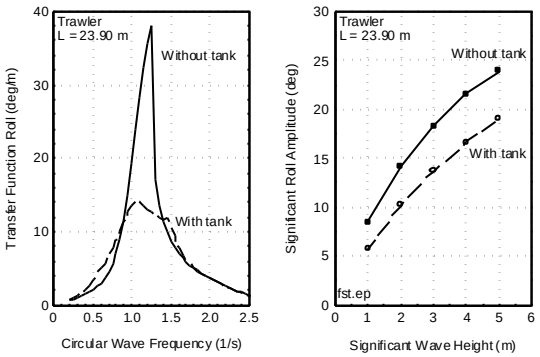

Figure 7 Effect of Free-Surface Anti-Roll Tank on Roll

Figure 7 shows an example of the reduction of the transfer function and significant amplitude of roll for a trawler, equipped with a free-surface anti-roll tank.

2.3.3 LNG Cargo Tank

Thirdly, forced roll oscillation experiments have been carried out with a 2-D model of a cargo tank of a LNG carrier. A sketch of this 1:25 model of the tank is given in Figure 8.

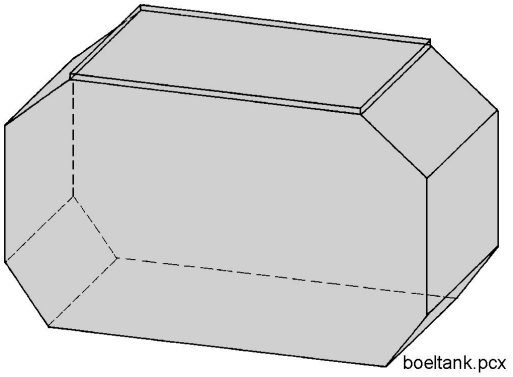

Figure 8 Model of an LNG Tank

At filling levels of 15, 45, 70, 90, 97.5 and 100 per cent of the depth of the tank, the exciting roll moments have been measured for a range of oscillation frequencies and one roll amplitude $\left(f_a = 0.10 = 5.7^0\right)$ of the tank. Because of the shape of this tank, a strong non-linear behavior was expected at the lowest and highest free-surface levels.
Figure 9 through Figure 14 show the measured and predicted in-phase and out-of-phase parts of the first harmonic of the roll moments of the LNG tank as a function of the frequency.

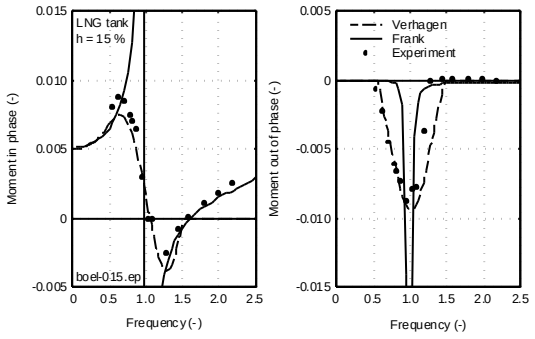

Figure 9 Roll Moments of an LNG Tank with 15 % Filling Level

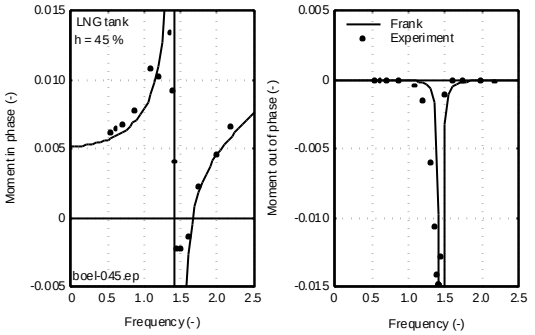

Figure 10 Roll Moments of an LNG Tank with 45 % Filling Level

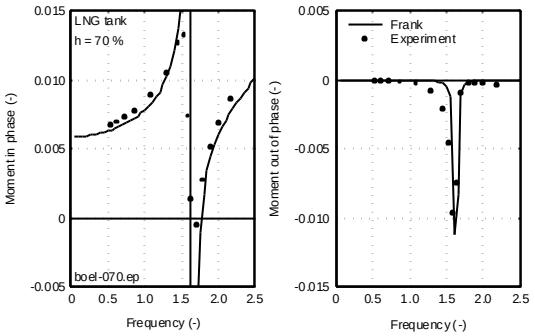

Figure 11 Roll Moments of an LNG Tank with 70 % Filling Level

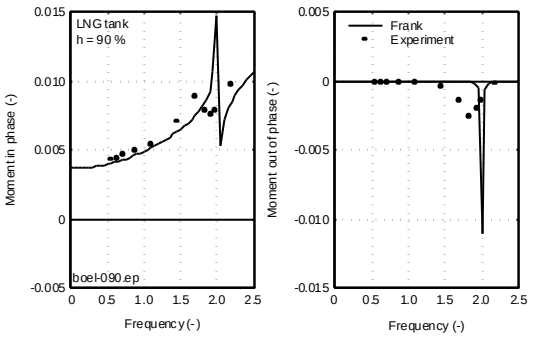

Figure 12 Roll Moments of an LNG Tank with 90 % Filling Level

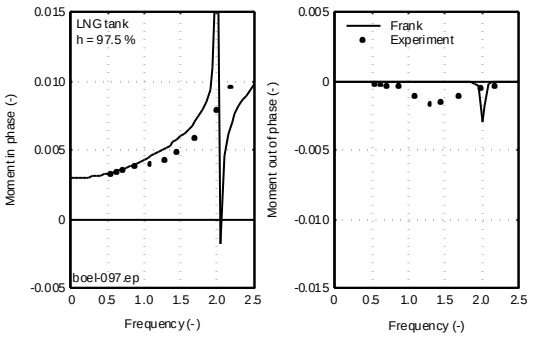

Figure 13 Roll Moments of an LNG Tank with 97.5 % Filling Level

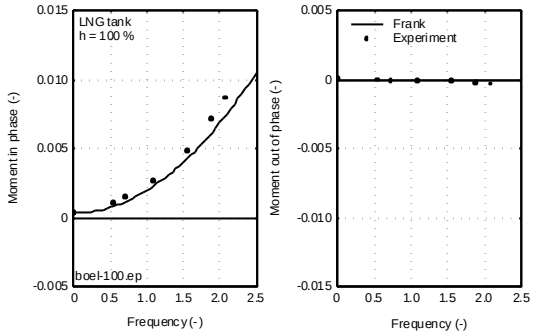

Figure 14 Roll Moments of an LNG Tank with 100 % Filling Level

The roll moment has been made non-dimensional by dividing this moment through $r\,\mathrm{glb}^3$. The non-dimensional frequency parameter has been obtained by dividing the frequency through $\sqrt{g/b}$.

Except at the natural frequency of the fluid in the tank, a fairly good prediction has been found with Frank's method.

Again, the shallow water method of Verhagen and Van Wijngaarden gives a good prediction for all frequencies at the lowest filling level of the tank.

Effect on Ship Motions

To investigate the effect of free surface (liquid cargo) tanks on the roll motions of a ship, three tanks as given in Figure 8 were build in a 1:60 model of an LNG carrier. The body plan of this vessel is given in Figure 15.

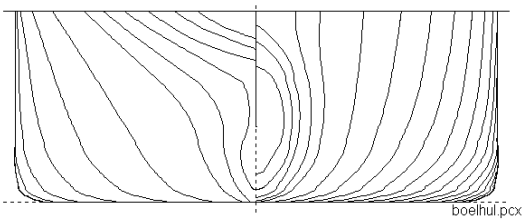

Figure 15 Body Plan of LNG Carrier

Static heel tests and roll decay tests in still water and roll motion measurements in regular beam waves with two different wave amplitudes were performed at zero forward ship speed. The model was placed transversal in the towing tank at half the length of the tank and the spacing between the model and the tank walls was about 0.70 meter. The model was free to move in 6 degrees of freedom and the roll damping waves could propagate over a long distance before they were reflected to the model by the tank-ends. The main dimensions of the ship are given in Table 1.

LNG Carrier			
Length bpp	L_{pp}	m	164.00
Breadth	B	m	32.24
Draught	d	m	12.60
Trim	t	m	0.00
Volume	∇	m^3	51680
Block coefficient	C_b	-	0.776
Length of bilge keels	l_{bk}	m	69.70
Height of bilge keels	h_{bk}	m	0.30
Gyradios for yaw	k_{zz}	m	45.43

Table 1 Main Dimensions of Ship

The length of each of the three cargo tanks was 13.45 meter and the distance of the bottom of the tanks above the ship's base line was 2.00 meter. With the exception of these amidships cargo tanks 3, 5 and 7, all other cargo tanks are supposed to be filled up to 97.5 per cent of the inner tank height with a stowage factor of 1.00 ton/m^3. This was simulated in the experiments by solid ballast weights and an adaptation of the radius of inertia for roll of the ship.

For the cargo tanks 3, 5 and 7 three loading conditions have been chosen:

- Condition I: frozen liquids (45-45-45%)
  The three cargo tanks are equally filled up to 45% of the inner tank height with homogeneous frozen liquid cargo with a stowage factor of 1.00 ton/m^3, simulated by solid ballast weights.
- Condition II: liquids (45-45-45%)
  This condition is similar to condition I after melting the cargo, so the three tanks are partially filled with water.
- Condition III: liquids (45-70-15%)
  This condition is similar to condition II, but the filling levels of the three tanks are 45%, 70% and 15%, respectively.

The results of the static heel angle tests and the roll decay tests are given in Table 2.

Condition		I	II	III
∇	m^3	51680	51680	51360
KG	m	10.48	10.42	10.60
GM	m	2.75	2.81	2.62
GG'	m	0.00	1.69	1.59
k_{xx}	m	10.14	9.38	9.49
$T_{\phi\text{-meas.}}$	s	13.70	21.30	23.00
$T_{\phi\text{-calc.}}$	s		21.18	22.82

Table 2 Loading Conditions

The measured non-dimensional roll damping coefficients k are presented in Figure 16.

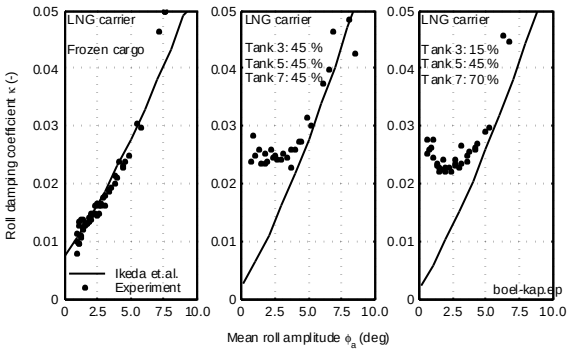

Figure 16 Roll Damping Coefficients

These data have been compared with predicted values obtained with the semi-empirical method of Ikeda.

For condition I, with frozen liquid cargo, a very good agreement has been found. For conditions II and III, with liquid cargo, the predicted roll damping coefficients are somewhat underestimated at smaller roll angle amplitudes. But at larger roll angle amplitudes, which are of interest in more dangerous circumstances, the figure shows a fairly good agreement.

Figure 17 and Figure 18 show a comparison of the measured and predicted roll amplitudes at two different wave amplitudes for each loading condition.

For loading condition I, the non-potential roll damping has been obtained by the method of Ikeda. The radius of inertia for roll of the ship's mass has been obtained from the measured natural roll period of 13.7 seconds and calculated hydromechanic coefficients. The figure shows a good agreement between experiments and predictions.

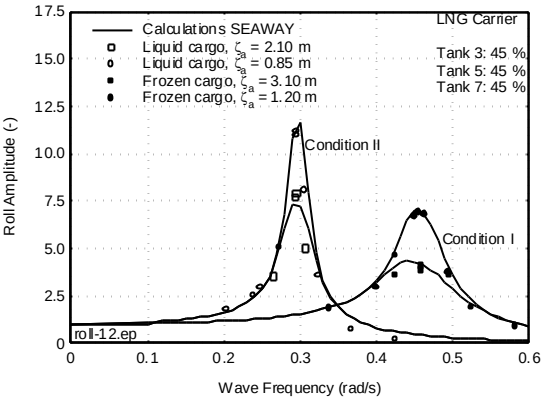

Figure 17 Roll Motions of LNG Carrier, Conditions I and II

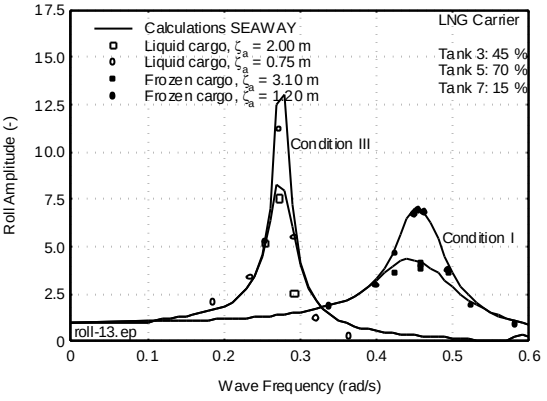

Figure 18 Roll Motions of LNG Carrier, Conditions I and III

For the loading conditions II and III, the non-potential roll damping has been obtained by the method of Ikeda (1978) too. The radius of inertia for roll of the ship's mass has been obtained from the radius of inertia of the ship with the frozen liquid cargo of condition I, after a correction for melting this cargo. The deviating volume of liquid cargo in condition III has been accounted for too. The exciting roll moments due to liquid cargo have been obtained with Frank's method.

So, for the loading conditions II and III, the roll motions have been calculated without using any experimental data of these loading conditions. Table 2 shows a very good agreement between the predicted and the

measured natural roll frequencies; the deviation is less than 1%. Figure 17 and Figure 18 show a very good agreement between the predicted and the measured response amplitude operators for roll.
However, it may be noted that for the loading conditions II and III, the natural roll frequency of the ship is about half the lowest natural frequency of the fluid in the three cargo tanks. When these frequencies are close to each other, non-linear effects caused by the bore or the hydraulic jump at the surface of the fluid in the tanks will play a much more important role.

3 Time Domain Approach

Generally, ship motion calculations can be carried out easily with frequency domain programs. But, as a result of the formulation in the frequency domain, any system influencing the behavior of the vessel should have a linear relation with the motions of the vessel. However, in a lot of cases there are several complications, which violate this linear assumption, for instance the non-linear viscous damping, forces and moments due currents, wind and anchoring, etc. Also, forces and moments due to a collision and the ingress of water afterwards may show a very strong non-linear behavior.
To include these non-linear effects, it is necessary to formulate the equations of motion in the time domain, which relates instantaneous values of forces, moments and motions. For this purpose, use has been made of work published by Cummins (1962) and Ogilvie (1964).

3.1 Cummins Equations

The floating vessel is considered to be a linear system with displacement and rotation velocities as input and reaction forces and moments of the surrounding water as output. The object is supposed to be at rest at time $t = t_0$. Then, during a short time Δt, an impulsive displacement Δx with a constant velocity V is given to this object:

$$\Delta x = V \cdot \Delta t$$

During this impulsive displacement, the water particles will start to move. When assuming that the fluid is non-viscous and free of rotation, a velocity potential Φ linear proportional to V, can be defined:

$$\Phi = V \cdot \Psi \quad \text{for: } t_0 < t < t_0 + \Delta t$$

where Ψ is a normalized velocity potential.
After this impulsive displacement Δx, the water particles are still moving. Because the system is assumed to be linear, the motions of the fluid, described by the velocity potential Φ, are proportional to the impulsive displacement Δx:

$$\Phi = c \cdot \Delta x \quad \text{for: } t > t_0 + \Delta t$$

where c is a normalized velocity potential.
The impulsive displacement Δx during the period $(t_0, t_0 + \Delta t)$ does not influence the motions of the fluid during this period only, but also further on in time. This holds that the motions during period $(t_0, t_0 + \Delta t)$ are influenced by the motions before this period too. When the object performs an arbitrarily with time varying motion, this motion can be considered as a succession of small impulsive displacements. Then, the resulting total velocity potential $\Phi(t)$ during the period $(t_n, t_n + \Delta t)$ becomes:

$$\Phi(t) = \sum_{j=1}^{6} \Big\{ V_{j,n} \cdot \Psi_j + \sum_{k=1}^{n} \big\{ c_j (t_{n-k}, t_{n-k} + \Delta t) \cdot V_{j,k} \cdot \Delta t \big\} \Big\}$$

where:

n	number of time steps
t_n	$t_0 + n \cdot \Delta t$

t_{n-k} $t_0 + (n-k)\cdot\Delta t$

$V_{j,n}$ j-th velocity component during period $(t_n, t_n + \Delta t)$

$V_{j,k}$ j-th velocity component during period $(t_{n-k}, t_{n-k} + \Delta t)$

Ψ_j normalized velocity potential caused by a displacement in direction j during period $(t_n, t_n + \Delta t)$

c_j normalized velocity potential caused by a displacement in direction j during period $(t_{n-k}, t_{n-k} + \Delta t)$

Letting Δt go to zero, yields:

$$\Phi(t) = \sum_{j=1}^{6} \left\{ \dot{x}_j(t) \cdot \Psi_j + \int_{-\infty}^{t} c_j(t-t) \cdot \dot{x}_j(t) \cdot dt \right\}$$

where $\dot{x}_j(t)$ is the j-th velocity component at time t.
The pressure in the fluid follows from the linearised equation of Bernoulli:

$$p = -r \frac{\partial \Phi}{\partial t}$$

An integration of these pressures over the wetted surface S of the floating vessel gives the expression for the hydrodynamic reaction forces and moments F_i. With n_i for the generalized directional cosine, F_i becomes:

$$\begin{aligned} F_i &= -\iint_S p \cdot n_i \cdot dS \\ &= \sum_{j=1}^{6} \left\{ \left(r \iint_S \Psi_j \cdot n_i \cdot dS \right) \cdot \ddot{x}_j(t) \right. \\ &\quad \left. + \int_{-\infty}^{t} \left(r \iint_S \frac{\partial c_j(t-t)}{\partial t} \cdot n_i \cdot dS \right) \cdot \dot{x}_j(t) \cdot dt \right\} \end{aligned}$$

When defining:

$$A_{i,j} = r \iint_S \Psi_j \cdot n_i \cdot dS$$

$$B_{i,j}(t) = r \iint_S \frac{\partial c_j(t-t)}{\partial t} \cdot n_i \cdot dS$$

the hydrodynamic forces and moments become:

$$F_i = \sum_{j=1}^{6} \left\{ A_{i,j} \cdot \ddot{x}_j(t) + \int_{-\infty}^{t} B_{i,j}(t-t) \cdot \dot{x}_j(t) \cdot dt \right\}$$

for $i = 1,6$

Together with linear restoring spring terms $C_{i,j} \cdot x_j$ and linear external loads $X_i(t)$, Newton's second law of dynamics gives the linear equations of motion in the time domain. When replacing in the damping term t by $t-t$, this term can be written in a more convenient form. Then, the linear equations of motion in the time domain are given by:

$$\begin{aligned} &\sum_{j=1}^{6} \{ \left[M_{i,j} + A_{i,j} \right] \cdot \ddot{x}_j(t) + \\ &+ \int_{0}^{\infty} B_{i,j}(t) \cdot \dot{x}_j(t-t) \cdot dt + \\ &+ C_{i,j} \cdot x_j(t) \} = X_i(t) \end{aligned}$$

for $i = 1,6$

where:

$x_j(t)$ displacement or rotation in direction j at time t

$M_{i,j}$ solid mass or inertia coefficient

$A_{i,j}$ hydrodynamic mass or inertia coefficient

$B_{i,j}$ retardation function

$C_{i,j}$ spring coefficient

$X_i(t)$ external load in direction i at time t

Referring to the classic work on this subject by Cummins (1962), these equations of motion are called the Cummins Equations.

The linear restoring spring coefficients $C_{i,j}$ can be determined easily from the underwater geometry and the location of center of gravity G of the vessel, but to determine $A_{i,j}$ and $B_{i,j}$, the velocity potentials Ψ_j and c_j have to be found, which is very complex in the time domain. However, Ogilvie (1964) gives a much more simple method. He found these coefficients from the hydrodynamic mass and damping data, by using results of the linear 2-D or 3-D potential theory in the frequency domain. Relative simple relations are found between $A_{i,j}$ and $B_{i,j}$ and these frequency domain potential coefficients.

In Ogilvie's approach, the vessel is supposed to carry out a harmonic oscillation in the direction j with normalized amplitude: $x_j = 1 \cdot \cos(wt)$. After substitution of $x_j, \dot{x}_j$ and $\ddot{x}_j$ in the Cummins equations and comparing the time domain and the frequency domain equations, both with linear terms, he found:

$$A_{i,j} - \frac{1}{w}\int_0^\infty B_{i,j}(t) \cdot \sin(wt) \cdot dt = a_{i,j}(w)$$

$$\int_0^\infty B_{i,j}(t) \cdot \cos(wt) \cdot dt = b_{i,j}(w)$$

$$C_{i,j} = c_{i,j}$$

where:

$a_{i,j}(w)$ frequency-dependent hydrodynamic mass or inertia coefficient

$b_{i,j}(w)$ frequency-dependent hydrodynamic damping coefficient

$c_{i,j}$ spring coefficient

The first expression with mass terms is valid for any value of w, so also for $w = \infty$. Then the term with the integral, which will be divided by w, vanishes. This gives for the potential mass coefficient:

$$A_{i,j} = a_{i,j}(w = \infty)$$

A Fourier re-transformation of the second expression, with the damping term, gives the retardation function:

$$B_{i,j}(t) = \int_0^\infty b_{i,j}(w) \cdot \cos(wt) \cdot dt$$

Figure 19 shows an example of the retardation function for roll of a ship.

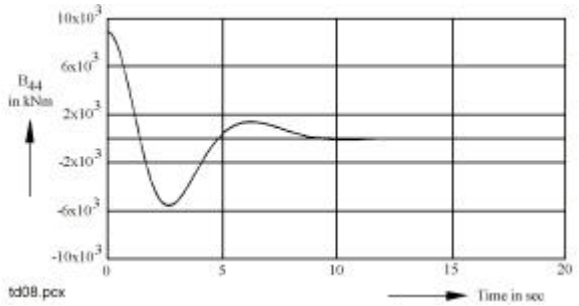

Figure 19 Retardation Function for Roll

The numerical problems that have to be solved, because of the integration has to be carried out from 0 to ∞, are not discussed here.

So far, discussion has concentrated on the left-hand side of the equations. Notice that this part of the equation is still linear. Attention shifts now to the right hand side, the external force $X(t)$. Since it can be convenient to keep the left hand side of the equation of motion linear, one often moves all the nonlinear effects - even a nonlinear damping or spring force - to the opposite side, where they are all considered to be part of the external force $X(t)$. Obviously one will have to know (or at least be able to evaluate) $X(t)$ in order to obtain a solution to the equation of motion.

Since the first order wave force is a linear phenomenon, time histories of the first order wave loads in a certain sea state can be

obtained from frequency domain calculations by using the frequency characteristics of the first order wave loads and the wave spectrum by using the superposition principle:

$$z(t) = \sum_{n=1}^{N} \left\{ z_{a_n} \cdot \cos(w_n t + e_n) \right\}$$

with randomly chosen phase shifts, e_n, between 0 and $2p$ and:

$$z_{a_n} = \sqrt{2 \cdot S_z(w) \cdot \Delta w}$$

which follows from:

$$\frac{1}{2} z_{a_n}^{\ 2} = S_z(w) \cdot \Delta w$$

With this, the time history of the first order wave load then becomes:

$$X_w(t) = \sum_{n=1}^{N} \left| \frac{X_{wa_n}}{z_{a_n}} \right| \cdot z_{a_n} \cdot \cdot \cos(w_n t + e_n + e_{X_w z_n})$$

where:

$X_w(t)$	wave load
N	number of frequencies
w	wave frequency (rad/s)
X_{wa_n} / z_{a_n}	transfer function of wave load (N/m)
$e_{X_w z_n}$	phase shift of wave load (rad)
e_n	phase shift of wave (rad)

Note that with a constant frequency interval, Δw, this time history repeats itself after $2p / \Delta w$ seconds.
With known coefficients and the right hand side of this equation of motion, it can be integrated a numerically. Comparisons of calculated and transformed linear motions in the frequency domain with time domain results show a perfect agreement.
It should be mentioned that, with this approach of Ogilvie (1964), the coefficients on the left-hand side of the Cummins equations are still linear.
But, the external loads $X_i(t)$ in the right hand side of the equations may also have a non-linear behavior now. For instance, a non-linear roll damping terms can be added.

3.2 Impulsive External Loads

A series of simple model experiments have been carried out to validate the time domain calculation routines with non-linear terms. Towing tank number 2 of the Delft Ship Hydromechanics Laboratory with a 1:40 model of the Oil Skimming Vessel m.v. Smal Agt (51.00 x 9.05 x 3.25 meter) was used for this. Horizontal impulse forces in the longitudinal and lateral direction have been introduced in a tow line between a torque-motor and the model in still water. The measured motions of the ship model have been compared with the data calculated in the time domain, using the measured time-series of the impulse forces and assumed points of application as an input. An example of the comparison is presented in Figure 20 the sway velocities due to a lateral impulse force amidships.

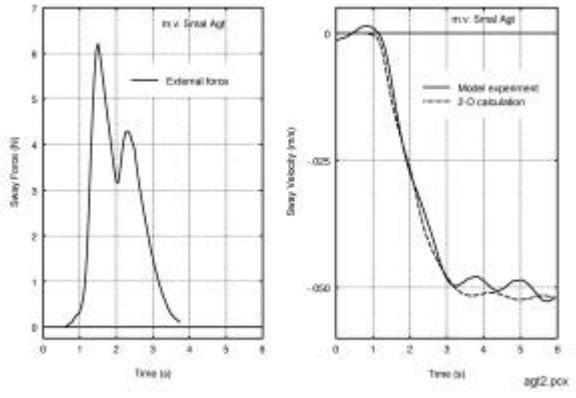

Figure 20 External Impulse and Resulting Motions

The figure shows a good agreement between the calculated and the measured sway motions. Comparable agreements have been found for the other tests.
A few years ago, the Centre for Applied Research in The Netherlands (TNO) carried out a series of full scale collision tests with two inland waterway tankers in still water, see Figure 21.

Figure 21 Under Water Portion of Rammed Ship

The contact forces between the two ships and the motions of the rammed ship were measured. Computer simulations of the motion behavior of the rammed ship during the collision have been carried out, using the measured contact forces on the rammed ship as an input.
Figure 22 shows some comparative results for a test with a collision of the rammed ship at about $0.40 \cdot L_{pp}$ from the bow on the port side. The ramming ship had a speed of about 15 km/hr. The measured and calculated motions of the rammed ship are presented. Sway, roll and yaw velocities are predicted here very well.

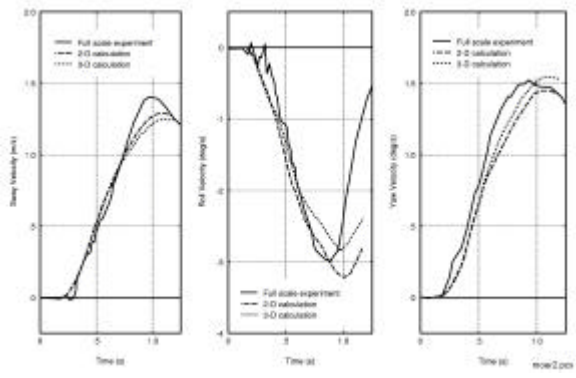

Figure 22 Velocities during a Ship Collision

3.3 Ingress of Water

Now the Cummins equations will be extended with terms describing the ingress of water.

3.3.1 Ingress Loads

The inclining moment is caused by the weight of the floodwater present in the flooded compartments. Throughout the flooding process and the consequential heeling of the vessel both, the amount of water and its location of the center of gravity, vary.
In general, the contribution of the weight of the floodwater to the inclining moment in a particular compartment can be written as:

$$X_4 = rgv \cdot (y \cos f + z \sin f)$$

where (see also Figure 23):

X_4	inclining moment due to weight of water in a compartment
r	density of flood water
g	acceleration of gravity
v	volume of water in compartment
y	transverse distance between c.o.g. and center line, measured parallel with the ship's base line
z	vertical distance between c.o.g. and base line, measured parallel with the ship's center line
f	heel angle

The total inclining moment equals the sum of the moments of each flooded compartment.

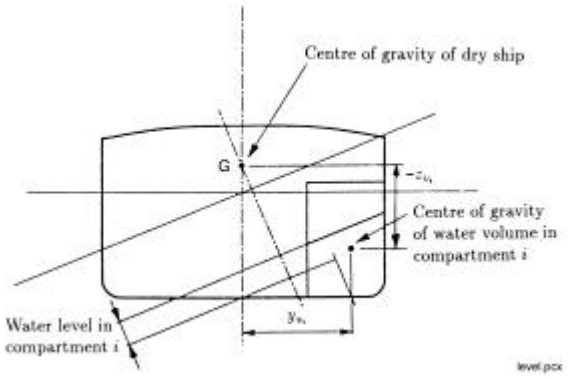

Figure 23 Definition of Symbols

The inclining moment, as described above, refers to the intersection of the ship's center plane and the base plane. The equations of motion of the ship refer to the ship's center of gravity. Therefore, a correction must be applied on this moment:

$$X_{4cog} = X_4 \cdot z_{cog} \cdot \cos f$$

where:

X_{4cog}	inclining moment due to weight of water in a compartment with respect to the ship's c.o.g.
z_{cog}	vertical distance between c.o.g. and base line, measured parallel with the ship's center line

The amount of floodwater in each compartment depends on the flow of water and flow of air through the damage orifices and the cross-flooding openings. In case of wing compartments, the effect of air vents has to be taken into account.
Water flow can be calculated by applying Bernoulli's law:

$$Q_{water} = A\sqrt{\frac{2 \cdot \Delta P}{r \cdot C}}$$

where:

Q_{water}	flow rate between sea and damaged compartment or between adjacent flooded compartment
A	flow area
ΔP	pressure difference over ingress opening c.q. flooding connection between compartments
C	coefficient accounting for flow resistance due to inlet-outlet effects, friction, etc.

For reference, it must be noted that the relation between the coefficient C and the pressure loss coefficient F, as applied in the explanatory notes issued by IMO, can be written as:

$$F = \frac{1}{\sqrt{C}}$$

The airflow can be calculated in a similar manner, however the formula is slightly more complicated due to the compressibility of the air:

$$Q_{air} = A\sqrt{\frac{2 \cdot R \cdot T \cdot \Delta P}{\left|P_f + P_r\right| \cdot C}}$$

with:

Q_{air}	flow rate of air through vents
A	flow area
R	specific gas constant of air
T	temperature of air
ΔP	pressure difference over air vent
P_f	pressure at front of air vent
P_r	pressure at rear of air vent
C	coefficient accounting for flow resistance due to inlet-outlet effects, friction, etc.

In the case of the ingress openings and the cross-flooding openings two complications occur. The pressure head varies along the height of the opening and the water levels may lie between the upper and lower edge of the opening. Dividing the opening vertically into a number of strips can cater for these complications. It can be decided per strip whether water flow or air flow occurs.

Flow is assumed to stop when the pressure difference over an orifice, flow opening or air vent becomes zero. This happens when water levels in adjacent compartments are equal, which can only occur when these compartments extend vertically above the damaged water line.
In case of a compartment, which is located fully below the damaged water line, it is assumed that some air (10% of total compartment capacity) remains trapped inside the compartment. To calculate the air pressure in this trapped volume, the simple gas law is applied:

$$Q_{air} = \frac{R \cdot T}{V_{air}}$$

where:

P_{air} air pressure
V_{air} volume of trapped air

3.3.2 Model Experiments

The main dimensions of the full size vessels are given in Table 3. The scale of the two models was 1:50.

		Ferry-62	Ferry-72
Length over all	m	161.00	179.30
Length b.p.p.	m	146.40	169.20
Moulded breadth	m	27.60	24.92
Depth Ro-Ro deck	m	8.10	7.85
Draught	m	6.22	6.08
Clock coefficient	-	0.617	0.717
Volume	m^3	15,500	18,375
1.20 x GM	m	-	1.92
1.00 x GM	m	2.05	1.60
0.80 x GM	m	1.64	1.28
0.60 x GM	m	1.23	-

Table 3 Principal Dimensions of Ship

The models were positioned in a transverse manner in the towing tank at half the length of the tank. The distance between the models and the tank walls was about half a meter and the roll damping waves could propagate over a long distance before they were, after reflection by the tank-ends, diffracted to the model.

Experimental Set-Up
During the experiments, the roll motions of the model were measured on time basis. The sign of these data corresponds to a right-handed orthogonal coordinate system with the origin in the center of gravity G of the ship, the x-axis in the longitudinal forward direction, the y-axis to port side and the z-axis upwards. This means that heel or roll to starboard is positive and heel or roll to port side, so to the gap, is negative.
The shape of the collision gaps is based on the result of a collision in the side by a ship with a bulbous bow, so a circular gap under the waterline and a triangular gap above the waterline. The shape and the full-scale dimensions (in mm) of the four collision gaps in the ship are presented in Figure 24. The reference line for the vertical measures in this figure is the ship's base line.

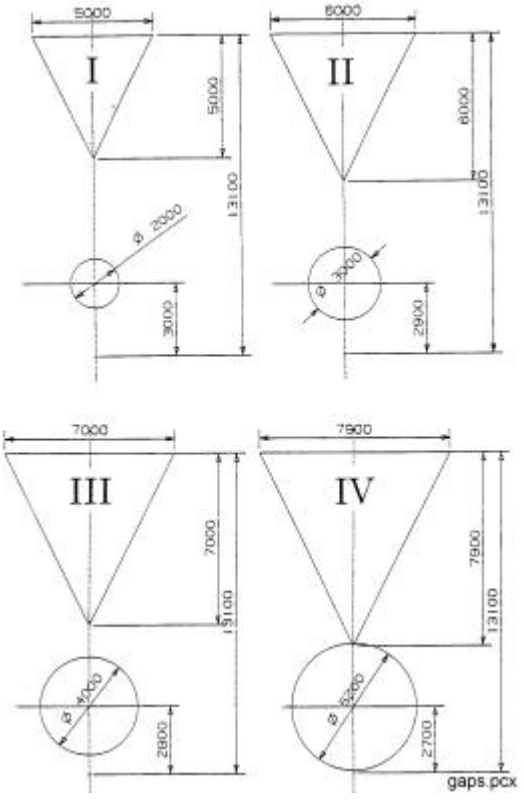

Figure 24 Collision Gaps

The projected areas of these gaps are given in Table 4.

Gap No.	Projected Gap Area		
	Circle (m^2)	Triangle (m^2)	Total (m^2)
I	3.14	12.50	15.64
II	7.07	18.00	25.07
III	12.57	24.50	37.07
IV	21.24	31.20	52.44

Table 4 Areas of Collision Gaps

The time histories of the roll angles during the sudden ingress of water into the model are presented. A while before opening the gap the registration was started and a time-reference signal was made available to obtain the instant of opening the gap, $t = 0$.
As soon as the port side gap is opened, water will flow into the model and the port side pressure on the model at the gap will drop down. Still, the effect of the in-flooding water has to start. At the starboard side of the model the static water pressure on the model maintains. During a short time, this results in a total hydrostatic force to port side. Because the gap is below the center of gravity, this force causes a small initial roll to starboard. After that, the effect of the flooding water will increase and the model starts to roll to port side.
The experiments were carried out in such a way that the effect of the growth of the gap after the collision with time on the ship motions could be neglected. So, the gap came into existence very sudden; it was nearly a step function. The gap in the hull of the model was closed by a flexible rubber flap, sticked with vaseline to the outside exterior of the hull around the gap.
Without introducing a roll moment, the flap was catapulted away backwards by a spring construction on the model. The release of the sealed spring took place electrically, without touching the model. Experiments on catapulting away the flap from the model without a gap, showed that the discharge of the energy in the spring construction and the slight disturbance of the still water surface by the moving flap did not result in significant ship motions.
Each experiment has been started with a dry model. Water leaked between the flap and the hull via the gap into the model, if any, was pumped away just before starting the experiment. To examine the repeatability of the experimental results, a large number of experiments have been carried out twice or even three times.

Experiments Ferry-62
The bodylines of Ferry-62, the engine rooms with bulkheads and spaces and the location of the collision-gaps are shown in Figure 25. The transverse bulkhead between the engine rooms was at half-length of the gap. Wooden blocks modeled the engines.

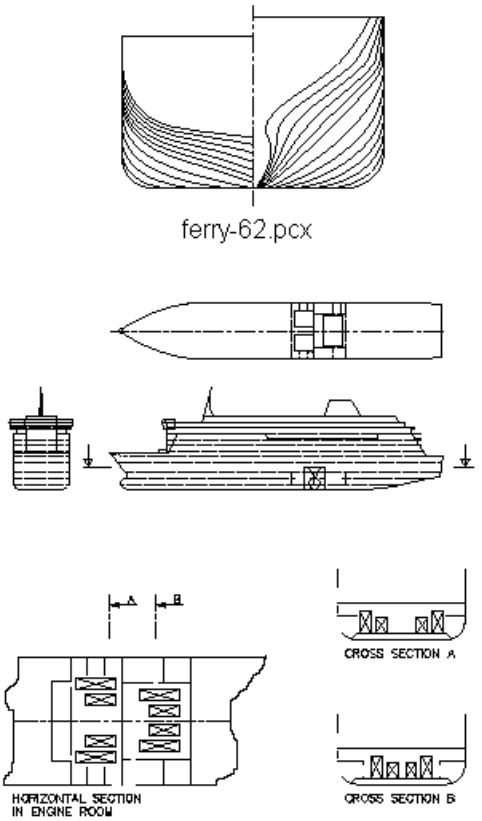

Figure 25 Ferry-62

The experiments were carried out at three different values for the initial metacentric height. The values of $\overline{GM}$-ship were 2.05 meter (100%), 1.64 meter (80%) and 1.23 meter (60%), respectively.

To obtain roll-damping information, free rolling experiments were carried out with the intact model, so the model with a closed gap, and with the flooded model with gap I.
Then, capsize tests were carried out for the three metacentric heights and the four gaps. To examine the effect of a small initial heel angle, these experiments were repeated with an initial heel.
To examine the effect of the free surface of the flooded water on the Ro-Ro deck, the experiments, which resulted into capsizing, were repeated with a reduced deck width.

Roll Decay Tests Ferry-62

For three metacentric heights of Ferry-62, free rolling experiments were carried out with the intact model, so the model with a closed gap, and for the flooded model with gap I. The $\overline{GM}$ value of the intact ship, the heeling moments corresponding to the initial heel angles, the measured natural roll periods T_f and the gyradii for roll of the ship k_{ff}, obtained from T_f, are given in Table 5.

Intact Ship				Ship / Gap I	
$\overline{GM}$		T_f	k_{ff}/B	T_f	k_{ff}/B
(m)	(%)	(s)	(-)	(s)	(-)
2.05	100	15.3	0.395	15.3	0.395
1.64	80	17.0	0.395	19.3	0.445
1.23	60	19.2	0.385	20.4	0.410

Table 5 Still Water Results of Ferry-62

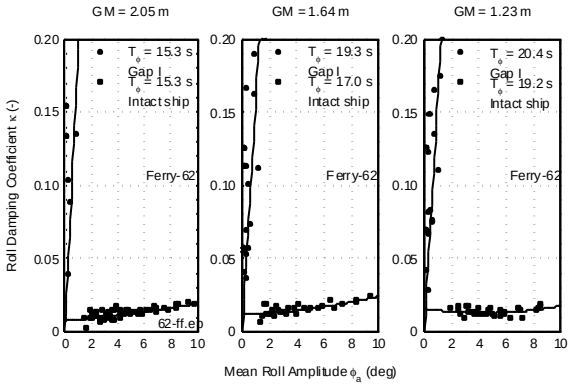

Figure 26 Roll Damping of Ferry-62

The non-dimensional rolldamping coefficients $k(f_a)$ are presented in Figure 26. The figure shows a considerable increase of the roll damping during flooding of the engine rooms of the ship. The obstacles in the engine rooms, the simplified wooden models of the engines, mainly cause this.

Capsize Tests Ferry-62

When not taking into account the sinkage during flooding, the Ro-Ro deck of Ferry-62 enters into the water at a heel angle of 7.8 degrees.
The capsize tests were carried out at the three metacentric heights of 1.23, 1.64 and 2.05 meter and the four gaps I, II, III and IV. To examine the effect of a small initial heel angle, these experiments were repeated with initial heel angles of the ship. Without an initial heel, the ship capsized for all gaps within 7 minutes at the lowest $\overline{GM}$ of 1.23 meter (60%) and survived at the other $\overline{GM}$ values. But with an initial heel angle of about -3 degrees, the ship capsized in all examined cases. At a $\overline{GM}$ of 1.64 meter (80%), the ship capsized when the initial heel angle was about -1 degrees. At the actual $\overline{GM}$ of 2.05 meter, the ship capsized when the initial heel angle was about -3 degrees. The duration of capsizing is strongly depending on the size of the gap; at the largest $\overline{GM}$, 7 minutes for gap I and 1 minute for gap IV.

For the largest gap, an example of the results is presented in Figure 27.

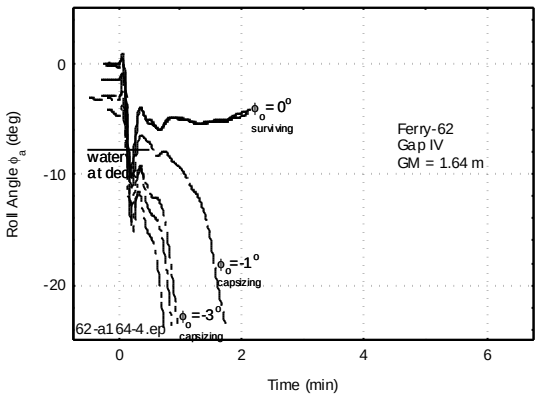

Figure 27 A Capsize Result of Ferry-62

To examine the effect of the free surface of the flooded water on the Ro-Ro deck, those experiments, which resulted into capsizing, were repeated at a reduced deck width. Two beams of hard foam at the Ro-Ro deck at port side and at starboard, with a breadth of 2.50 meter simulated this. This modification did not result into an avoidance of capsizing. However, the time necessary for capsizing will be increased by about 50 per cent. An example is given in Figure 28.

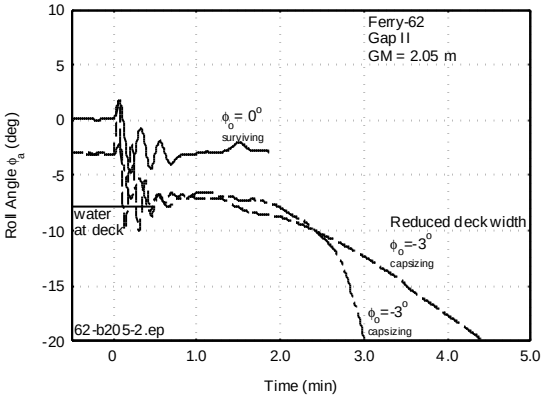

Figure 28 Influence of Reduced Deck Width on Capsizing of Ferry-62

Experiments Ferry-72

The body lines of Ferry-72, the engine rooms with cross ducts, bulkheads and spaces and the location of the collision-gaps are shown in Figure 29.

The transverse bulkhead in the side at half the length of the engine room was in the middle of the gap. During the tests, the engine room was empty.

The experiments were carried out at three different values for the initial metacentric height. The values of $\overline{GM}$-ship were 1.92 meter (120%), 1.60 meter (100%) and 1.28 meter (80%), respectively.

To obtain roll-damping information, free rolling experiments were carried out with the intact model, so the model with a closed gap, and with the flooded model with gap I.

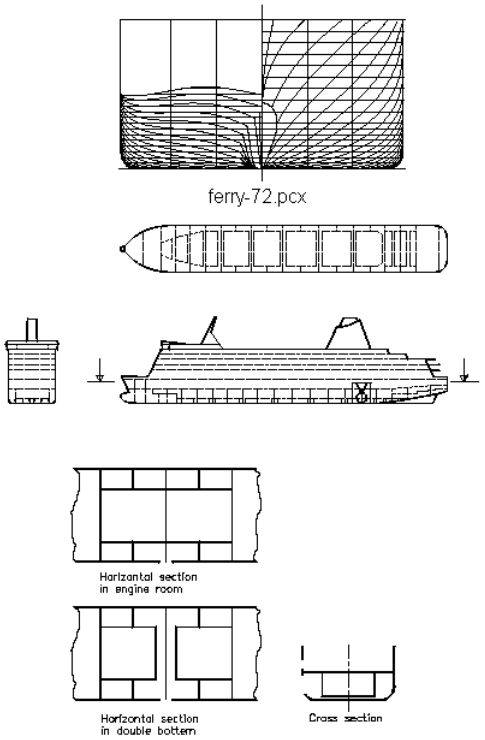

Figure 29 Ferry-72

Then, a series of capsize tests were carried out for the three metacentric heights and the four gaps. To examine the effect of a small initial heel angle, these experiments were repeated with an initial heel.

To examine the effect of the longitudinal bulkheads, also capsize tests were carried out with the model without these bulkheads, so with engine rooms over the full breadth of the ship.

To examine the effect of the cross duct in the double bottom, capsize tests were carried out with the model with a closed duct.

To examine the effect of water on the Ro-Ro deck, some experiments, which resulted into capsizing, were repeated with deck openings in the Ro-Ro deck.

A few experiments were carried out with the model without a cross duct but with 60 per cent of the volume hard foam in the two port side wing tanks.

Finally, some experiments were carried out in regular beam waves with an amplitude of 1.0 meter.

Roll Decay Tests Ferry-72

For the metacentric heights of Ferry-72, free rolling experiments were carried out with the intact model, so the model with a closed gap, and for the flooded model with gap I. The $\overline{GM}$ value of the intact ship, the heeling moments corresponding to the initial heel angles, the measured natural roll periods T_f and the longitudinal gyradii for roll k_{ff}, obtained from T_f, are given in Table 6.

Intact Ship				Ship / Gap I	
$\overline{GM}$		T_f	k_{ff}/B	T_f	k_{ff}/B
(m)	(%)	(s)	(-)	(s)	(-)
1.92	120	14.5	0.400	13.8	0.380
1.60	100	16.2	0.410	15.1	0.380
1.28	80	18.4	0.415	17.3	0.390

Table 6 Still Water Results of Ferry-72

The non-dimensional roll-damping coefficients $k(f_a)$ are presented in Figure 30.

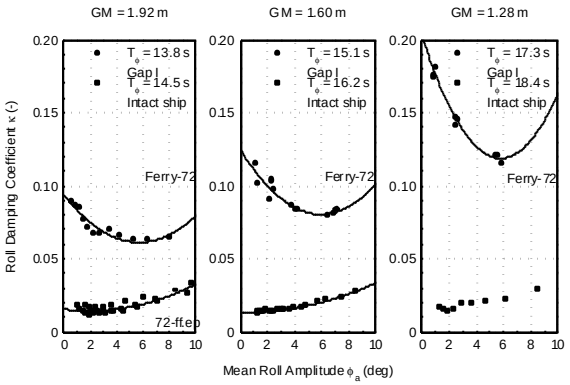

Figure 30 Roll Damping of Ferry-72

The figure shows an increase of the roll damping during flooding of water in the ship. The roll damping increases with the metacentric height.

Capsize Tests Ferry-72

When not taking into account the sinkage during flooding, the Ro-Ro deck of Ferry-72 enters into the water at a heel angle of 8.1 degrees.

The capsize tests were carried out at the three metacentric heights of 1.28, 1.60 and 1.92 meter and the four gaps I, II, III and IV. To examine the effect of a small initial heel angle, these experiments were repeated with an initial heel.

Without an initial heel angle, the ship survived in all cases. With an initial heel angle of -3 degrees and the smallest gap, the ship survived too. But with the largest gap, the ship capsized within 1.5 minutes for the lowest $\overline{GM}$ of 1.28 meter (80%) and it survived at the higher $\overline{GM}$ values. With an initial heel angle between -4 and -5 degrees, the largest collision gap and the actual $\overline{GM}$ of 1.60 meter, the situation became critical. The ship hesitated to capsize or it capsized within 2.5 minutes.

For the largest gap, an example of the results is presented in Figure 31.

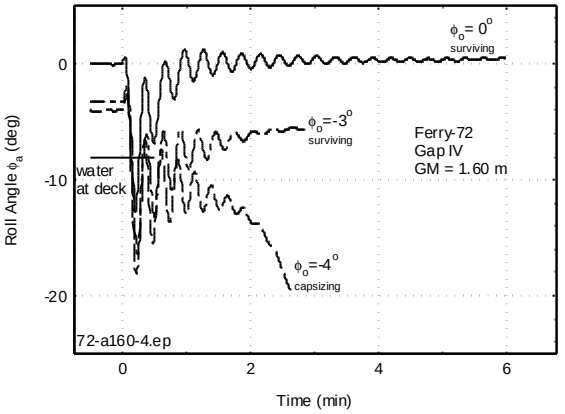

Figure 31 A Capsize Result of Ferry-72

To examine the effect of the longitudinal bulkheads in the engine room on the safety of the ship, also the time histories of the roll angles were measured during a flooding of the Ferry-72 model without these longitudinal bulkheads, see Figure 32.

After opening the gap with a zero initial heel angle of the ship, an extreme roll angle of -9 degrees was reached and some water entered on the Ro-Ro deck. Then the ship returned oscillating to an upright position and it seemed to survive. But, due to the water flooding into the engine room, the ship sunk horizontally. As soon as the metacentric height became negative, the ship started to

heel to starboard and finally it capsized after 7 minutes.

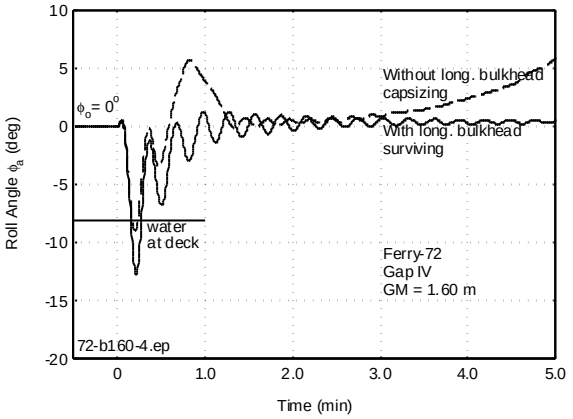

Figure 32 Influence of Longitudinal Bulkhead on Capsizing of Ferry-72

In these model experiments, the ship capsized to starboard because it had a small initial heel to starboard during horizontal sinkage. This was caused by a small loss of port side mass of the rubber flap and the springs after catapulting away the flap.

To examine the effect of the cross duct in the double bottom, capsize tests were carried out with a closed cross duct. Some results are presented in Figure 33 for the actual $\overline{GM}$ of 1.60 meter and the smallest collision gap.

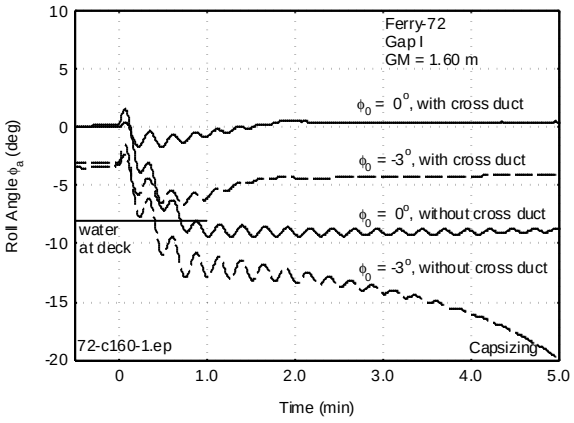

Figure 33 Influence of Cross Duct on Capsizing of Ferry-72

With a cross duct and no initial heel, the ship remained safe. With an initial heel angle of -3 degrees, the ship survived with a final heel angle of -4 degrees, due to a negative initial metacentric height.

With a closed cross duct and no initial heel, the ship survived with a final heel angle of -9 degrees, due to a negative initial metacentric height and the amount of water in the port side wing tanks. Some water entered to the Ro-Ro deck, so this became a very dangerous condition.

With a closed cross duct and an initial heel angle of -3 degrees, the ship capsized in 5 minutes.

A few experiments were carried out with the ship without a cross duct but with 60 per cent of the volume hard foam in the two port side wing tanks.

The results are presented in Figure 34 for the actual $\overline{GM}$ of 1.60 meter and the largest collision gap. The ship remained safe with a cross duct. Without a cross duct, the ship capsized after 3.5 minutes. But, with 60 volume per cent hard foam in the port side wing tanks, the ship remained safe with a final heel angle of -3 degrees.

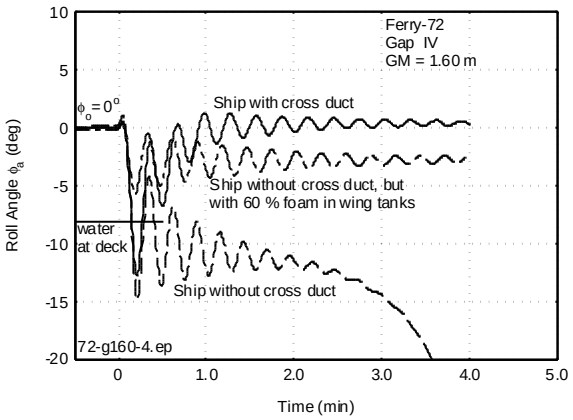

Figure 34 Influence of Permeability of Wing Tank on Capsizing of Ferry-72

To examine the effect of water on the Ro-Ro deck, some experiments, which resulted into capsizing or nearly capsizing, were repeated with deck openings in the Ro-Ro deck, through which water at deck could flow downwards. For the lowest metacentric height and collision gap III, an example of the results is given in Figure 35.

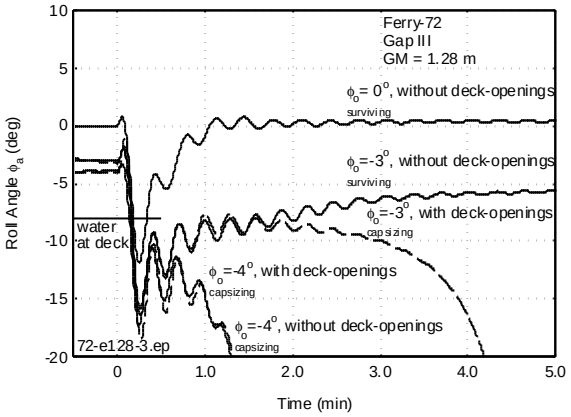

Figure 35 Influence of Deck Openings on Capsizing of Ferry-72

Without deck openings and no initial heel, the ship remained safe.
Without deck openings and with an initial heel angle of -3 degrees, the ship survived with a final heel angle of -6 degrees, due to a reduced metacentric height. With deck openings and with an initial heel angle of -3 degrees, the ship capsized after 4 minutes.
Without and with deck openings and an initial heel angle of -4 degrees, the ship capsized within 1.5 minutes.

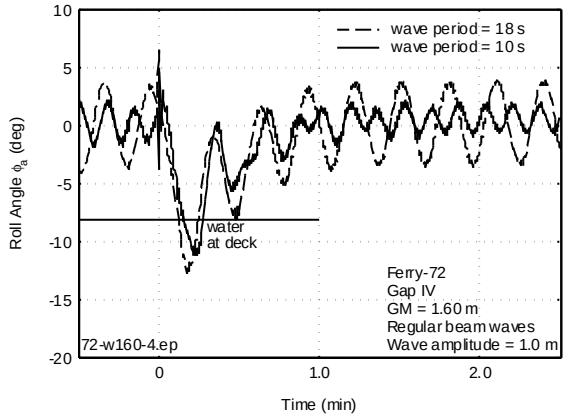

Figure 36 Influence of Regular Beam Waves on Capsizing of Ferry-72

Finally, experiments were carried out in regular beam waves with an amplitude of 1.0 meter and a wide range of wave periods. Figure 36 presents some results for the actual $\overline{GM}$ of 1.60 meter, the largest collision gap and two regular wave periods. In all wave conditions the ship remained safe.

3.3.3 Validation of Theories

The calculation method, as described in sections 2.1 and 2.2 and as implemented in the computer simulation program DYNING (DYNamic INGress of water), has been subjected to validation against model experiments. Unfortunately, no full-scale test data could be obtained until now. As a consequence, any scaling effects are ignored.

Prior to validation against some of the tests as presented in this paper, a preliminary validation has been carried out based on tests with a pontoon type model of 3.00 meter length, 2.10 meter width and a draught of 0.625 meter. The model was fitted with opposite wing tanks, connected with a cross duct. The results of this validation study were satisfactory, as published by Vredeveldt and Journée (1991).

Figure 37 and Figure 38 show calculated and measured angles of roll for Ferry-62 due to sudden water ingress, obtained during a feasibility study of the tests described in this paper. These first model experiments on Ferry-62 are given in a limited distributed report by Journée (1994).

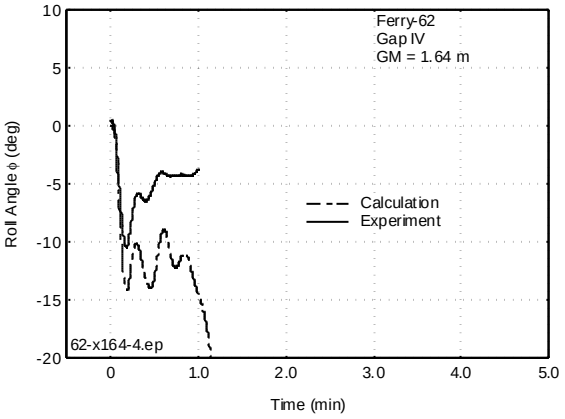

Figure 37 Measured and Calculated Roll of Ferry-62 for GM = 1.64 m

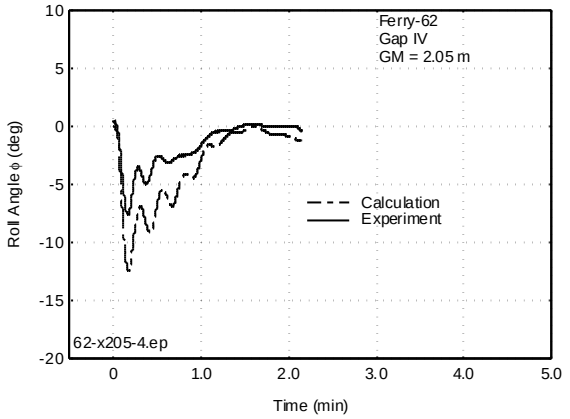

Figure 38 Measured and Calculated Roll of Ferry-62 for GM = 2.05 m

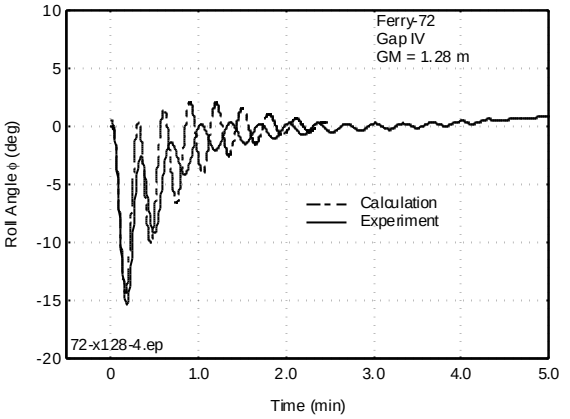

Figure 39 Measured and Calculated Roll of Ferry-72 for GM = 1.28 m

Figure 37 refers to a realistic $\overline{GM}$ value of 2.05 meter. Figure 38 shows results for a $\overline{GM}$ of 1.64 meter, which would normally not be accepted during operation.

As can be seen, the calculated time span till maximum heel correlates well with the measured value. However, the calculated angle of heel is larger than the measured value. Moreover, in this case the calculated decay is much smaller than measured. The best suggestion for an explanation of both differences is that the sloshing effect of the floodwater is too large to be neglected. However, it should be remarked that the chosen test case for the Ferry-62 does not take into account the presence of piping in the engine room, which is expected to have a large damping effect on the sloshing motions. Making any sensible remarks on this aspect seems impossible on the basis of theory and model experiments alone.

Figure 39 and Figure 40 show calculated and measured roll motions for the Ferry-72 due to sudden water ingress as presented in this paper.

Figure 39 refers to a $\overline{GM}$ value of 1.60 meter, which is realistic for this ship. Figure 40 refers to a $\overline{GM}$ of 1.28 meter, which is beyond operational limits.

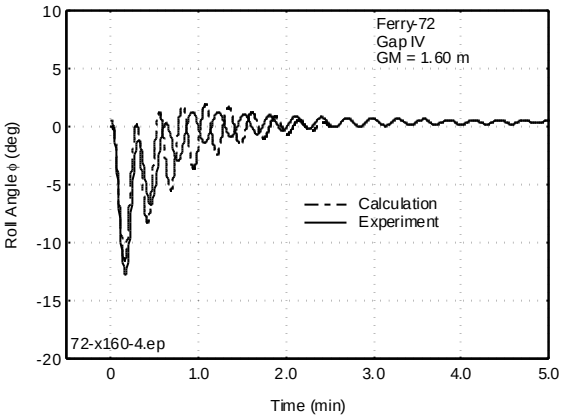

Figure 40 Measured and Calculated Roll of Ferry-72 for GM = 1.60 m

In this case calculated and predicted angle of heel and time required till maximum heel show a reasonable resemblance with measured values. However, again calculated motion decay is smaller than measured, although the difference is much smaller than in case of the Ferry-62.

The results support the suggestion that sloshing plays a significant role. In the test case of the Ferry-72 the sloshing motions of the floodwater will be much smaller than in case of the Ferry-62 because of the limited tank width of the flooded compartment, $1/5 \cdot B$ instead of $3/5 \cdot B$ in case of the Ferry-62.

4 Conclusions

From this variety of model experiments and calculations, some conclusions can be drawn.

Frequency Domain

From the calculations and the experiments in the frequency domain, the following conclusions may be drawn:

1. At very low filling levels of the tank, the method of Verhagen and Van Wijngaarden predicts the exciting roll moments fairly good. Because this theory is given for shallow water only, the method fails for higher filling levels.
2. With the exception of frequencies near to the natural frequency of the fluid in the tank, the potential theory of Frank predicts the exciting roll moments fairly good for all filling levels of the tank.
3. An addition of these roll moments in the right hand side of the equation of motions of the ship, results in good predictions of the roll motions of the ship.
4. The non-linear roll damping of the ship plays an important role in these roll motions. Linearisation results in a good prediction of the harmonic roll motions.

The pulsating source method of Frank, as included in many strip-theory ship motions computer programs, can be used easily to include the effect of non-viscous liquid cargo in ship motion calculations.

Also, 3-D calculation techniques for calculating potential mass and damping of ships can be used for this purpose.

Time Domain

The Cummins equations appear to be a very valuable tool for calculating ship motions in the time domain.

From the experiments with the Ferry-62 and the Ferry-72 in the time domain some conclusions may be drawn:

1. The roll decay tests show that obstacles like engines will cause a considerable increase of the roll damping of a ship in a flooded condition.
2. The experiments described in this paper showed that certain combinations of the $\overline{GM}$ value, the size of the collision gap and the magnitude of the initial heel angle can result in flooding of water on the Ro-Ro deck. As soon as this happens, a large probability on capsizing of the ship comes into existence.
3. It was found that the two longitudinal bulkheads in the engine room area of Ferry-72 were of paramount importance. Without these two bulkheads this ship will capsize, even at an upright initial condition. With an initial heel angle of -3 degrees, Ferry-72 with these bulkheads will survive while Ferry-62, not equipped with this type of subdivision, will capsize.
4. A cross duct has a very positive effect on the probability of survival of the ship. The restoring roll moment decreases, because water can flow in a short time from one side of the ship to the other side. Fitting obstacles in these ducts, like for instance pipes, should be avoided as far as possible.
5. The permeability of the wing tanks has a large effect on the probability of survival of the ship.
6. Deck openings in the Ro-Ro deck, through which water at deck can flow downwards, seemed to have a small negative effect on the safety of the ship. However, only one single case has been tested and the location of the deck openings is very important. So, this aspect needs further research.

For the Ferry-72 model the sloshing motions of the floodwater were much smaller than for the Ferry-62 model, because of the limited tank width of the flooded compartment of the first mentioned model. Sloshing was not included in the computer simulations in this paper. From the results of the simulations it appeared that a significant role of sloshing could be expected in the case of wide flooded compartments.

In the case of not too wide flooded compartments (Ferry-72), the roll motions predicted by the computer simulation

program DYNING are in a satisfactory agreement with the experimental data. But in the case of wide flooded compartments (Ferry-62) the agreement was very poor. This aspect needs further research too.

5 References

Van den Bosch and Vugts (1966)
J.J. van den Bosch and J.H. Vugts, *Roll Damping by Free Surface Tanks*, Report 83-S, 1966, NSRC-TNO, Delft, The Netherlands.

Cummins (1962)
W.E. Cummins, *The Impulse Response Function and Ship Motions*, Symposium on Ship Theory, January 25-27, 1962, Hamburg, Germany, Schiffstechnik, Vol. 9, Pages 101-109.

Frank (1967)
W. Frank, *Oscillation of Cylinders in or below the Free Surface of Deep Fluids*, Report 2375, October 1967, NSRDC, Washington D.C., U.S.A.

Ikeda, Himeno and Tanaka (1978)
Y. Ikeda, Y. Himeno and N. Tanaka, *A Prediction Method for Ship Rolling*, Report 00405, December 1978, Department of Naval Architecture, University of Osaka Prefecture, Japan.

Journée (1997)
J.M.J. Journée, *Liquid Cargo and Its Effect on Ship Motions*, 6th International Conference on Stability of Ships and Ocean Structures, September 22-27, 1997, Varna, Bulgaria.

Journée, Vermeer and Vredeveldt (1997)
J.M.J. Journée, H. Vermeer and A.W. Vredeveldt, *Systematic Model Experiments on Flooding of Two Ro-Ro Vessels*, 6th International Conference on Stability of Ships and Ocean Structures, September 22-27, 1997, Varna, Bulgaria.

Journée (1999)
J.M.J. Journée, *User Manual of SEAWAY, Release 4.18 (09-10-1999)*, Report 1213, 1999, Ship Hydromechanics Laboratory, Delft University of Technology, The Netherlands.

Journée and Massie (2000)
J.M.J. Journée and W.W. Massie, *Lecture Notes on Offshore Hydromechanics*, August 2000, Interfaculty Offshore Engineering, Delft University of Technology, The Netherlands.

Ogilvie (1964)
T. Ogilvie, *Recent Progress Towards the Understanding and Prediction of Ship Motions*, Proceedings of Fifth Symposium on Naval Hydrodynamics, Pages 3-128, September 10-12, 1964, Bergen, Norway.

Pinkster (1996)
J.A. Pinkster, *Hydrodynamic Aspects of Floating Offshore Structures*, Report 1050, May 1996, Ship Hydromechanics Laboratory, Delft University of Technology, The Netherlands.

Silverman and Abramson (1966)
S. Silverman. and H.N. Abramson, *The Dynamic Behavior of Liquids in Moving Containers, Edited by H.N. Abramson, Chapter 2: Lateral Sloshing in Moving Containers*, Report NASA SP-106, 1966, Scientific and Technical Information Division, National Aeronautics and Space Administration, Washington D.C., USA.

Verhagen and van Wijngaarden (1965)
J.H.G. Verhagen and L. van Wijngaarden, *Non-linear Oscillations of Fluid in a Container*, Journal of Fluid Mechanics, 1965, Volume 22, Part 4, Pages 737-751.

Vermeer, Vredeveldt and Journée (1994)
H. Vermeer, A.W. Vredeveldt and J.M.J. Journée, *Mathematical Modeling of Motions and Damaged Stability of Ro-Ro Ships in the Intermediate Stages of Flooding*, 5th International Conference on Stability of

Ships and Ocean Structures, 1994, Melbourne, U.S.A.

Vredeveldt and Journée (1991)
A.W. Vredeveldt and J.M.J. Journée, *Roll Motions of Ships due to Sudden Water Ingress, Calculations and Experiments, International Conference on Ro-Ro Safety and Vulnerability the Way Ahead,* April 17-19, 1991, London, U.K.

Vredeveldt, Journée and Vermeer (2000)
A.W. Vredeveldt, J.M.J. Journée and H. Vermeer, *The Effect of Crashworthiness and Solid Buoyancy on Survivability of Damaged and Flooded Ro-Ro Ships, 7*th International Conference on Stability of Ships and Ocean Structures, February 7-11, 2000, Launceston, Tasmania, Australia.